Published in final edited form as:
Nature. 2012 October 11; 490(7419): 219–225. doi:10.1038/nature11529.

Retinal waves coordinate patterned activity throughout the developing visual system

James B. Ackman[1], **Timothy J. Burbridge**[1], and **Michael C. Crair**[1]
[1]Department of Neurobiology, Yale University School of Medicine, New Haven CT, 06510

Summary

The morphologic and functional development of the vertebrate nervous system is initially governed by genetic factors and subsequently refined by neuronal activity. However, fundamental features of the nervous system emerge before sensory experience is possible. Thus, activity-dependent development occurring before the onset of experience must be driven by spontaneous activity, but the origin and nature of activity *in vivo* remains largely untested. Here we use optical methods to demonstrate in live neonatal mice that waves of spontaneous retinal activity are present and propagate throughout the entire visual system before eye opening. This patterned activity encompassed the visual field, relied on cholinergic neurotransmission, preferentially initiated in the binocular retina, and exhibited spatiotemporal correlations between the two hemispheres. Retinal waves were the primary source of activity in the midbrain and primary visual cortex, but only modulated ongoing activity in secondary visual areas. Thus, spontaneous retinal activity is transmitted through the entire visual system and carries patterned information capable of guiding the activity-dependent development of complex intra- and inter- hemispheric circuits before the onset of vision.

Introduction

The display of spontaneous activity is an emergent property of the immature nervous system that is thought to mediate synaptic competition[1] and instruct self-organization in many developing neural circuits[2,3,4]. If spontaneous activity is structured with respect to the topographic organization of first-order sensory and motor circuits, then these activity patterns could provide a template for activity-dependent development of downstream synaptic connectivity throughout the nervous system[5]. Whether spontaneous patterned activity exists and is communicated through all levels of organization for any sensory system during development is currently unknown.

In the developing visual system, isolated preparations of retina exhibit propagating bursts of action potentials among neighboring retinal ganglion cells (RGCs), termed ‘retinal waves’[6,7,8]. Since RGCs relay visual information to higher order structures in the central nervous system, retinal waves are thought to play a key role in the activity-dependent refinement of topographic neural maps in the superior colliculus (SC), dorsal lateral

Correspondence and requests for materials should be addressed to M.C.C. (michael.crair@yale.edu)..

Author Contributions J.B.A. and M.C.C. designed the experiments. J.B.A. performed *in vivo* ganglion cell axon, collicular neuron, and visual cortex imaging experiments and analyzed the recordings. T.J.B. performed intraocular ganglion cell labeling and *in vivo* ganglion cell axon imaging experiments and analyzed recordings. J.B.A. implemented analysis routines and analyzed the data. J.B.A. and M.C.C. wrote the manuscript.

The authors declare no competing financial interests.

Full methods and any associated references are available in the online version of the paper at www.nature.com/nature

Supplementary Information is linked to the online version of the paper at www.nature.com/nature.

geniculate nucleus (dLGN), and visual cortex[9,10,11,12,13], which exhibit functional connectivity before the onset of visual experience. However, the role of retinal waves in neural circuit development remains controversial[14,15], in part because their existence has never been demonstrated *in vivo*.

Previous work using extracellular microelectrode recording techniques *in vivo* demonstrated limited and local correlated spiking between pairs of embryonic rat RGCs[16], but no direct assessment of wave activity has been conducted *in vivo*, likely because of the methodological challenges associated with recording from a large cohort of RGCs in neonatal animals. In neonatal rat visual cortex, extracellular recordings show bursts of spiking activity and slow spreading oscillations that are sensitive to the presence of retinal input in the neocortex *in vivo*[17,18], but patterned spontaneous activity in and among different visual areas associated with retinal waves has never been observed. We sought to establish whether traveling waves of spontaneous retinal activity occur in neonatal mice *in vivo* and determine whether spontaneous retinal waves convey spatiotemporal patterns suitable for the activity-dependent refinement of visual maps throughout the nervous system before the onset of vision.

Spontaneous retinal waves occur *in vivo*

The most superficial layer of the mouse superior colliculus, the stratum griseum superficiale (SGS), receives retinotopically mapped terminal input from virtually all RGCs[19] and is completely accessible to imaging during development. We directly recorded from RGCs *in vivo* by injecting a calcium indicator, calcium green-1 dextran (CaGr-Dx), into the retina of neonatal mice and imaging the anterogradely labeled RGC axon arbors in the SC between three and nine days after birth (P3 – P9) through a cranial window using multiphoton or wide field fluorescence excitation (Fig. 1). Calcium imaging of RGC terminals revealed spontaneous waves of activity propagating throughout the SC of neonatal mice (Fig 1d-f and Supplementary Movie 1). Waves propagated among labeled RGC terminals at all depths examined within the SGS (range: 76 – 206 μm below the pial surface). Wave front velocity (median ± median absolute deviation: 44.17 ± 15.99 μm/s, N = 765 waves) was 3-4x slower than previously reported wave speeds measured in the mouse retina *in vitro*[20,21], which is consistent with the approximately 3x smaller diameter of the SC relative to the retina. Retinal waves occurred with a mean frequency (0.68±0.08 waves/min; N = 19 hemispheres) that was sensitive to age (Supplementary Fig. 1) and similar to the frequency observed *in vitro*[20,21]. Surprisingly, waves *in vivo* propagated over a much greater proportion of the SC area than was expected based on previous *in vitro* studies (median wave size ± median absolute deviation: 0.52 ± 0.30 mm^2, corresponding to ~30% of SC retinotopic area, compared with average wave size of ~1% of retina area *in vitro*[22]) (Supplementary Fig. 2). Waves were completely abolished after application of the Na^+ channel antagonist TTX into the contralateral eye (Fig. 1g-h and Supplementary Fig. 3) (N = 2 animals; ROI active fraction: control, 0.78±0.07; TTX, 0.00±0.00), but not the ipsilateral eye (N = 2 animals, ROI active fraction: control, 0.89±0.09; TTX, 0.999±0.001).

Retinal waves propagate to neurons in the superior colliculus

Most models for activity-dependent neural circuit development assume that patterned afferent activity drives target neuron spiking in order for Hebbian plasticity rules to strengthen synapses between coactive neurons. Previous work performed in an intact mouse retinogeniculate preparation *ex vivo* demonstrated that spontaneous retinal activity can drive dLGN neurons above spike threshold[23] and *in vivo* multielectrode recordings in the ferret showed that dLGN neurons exhibit correlated episodic bursting that was sensitive to ablation of retinal input[24] just before eye opening. However, it remains unknown whether

spontaneous retinal waves *in vivo* can actually drive wave-like network activity in RGC neural targets, a prerequisite for Hebbian refinement at developing synapses. We performed cellular-level calcium imaging in the SGS using bulk loading of the calcium indicator OGB1-AM (Fig. 2a-b) to determine whether retinal waves trigger traveling waves in retinorecipient neurons in the SC. Bolus indicator loading in the superficial layer of the SC labeled >1000 neurons within a 550×550 μm field of view (Fig. 2b-c). We first imaged at low power over the network of cells and neuropil as was done for calcium green-1 dextran imaging in Fig. 1. This revealed propagating calcium waves traveling within the retinorecipient layer of the SC (range: 34 – 172 μm below the pial surface) (Fig. 2d-f and Supplementary Movie 2). These waves occurred at the same frequency (0.69±0.17 waves/min, N = 11 hemispheres) as the retinal waves recorded presynaptically in RGC axons (p = 0.9497, t-test) (Supplementary. Fig. 1) and activated a similar percentage of the labeled area in the SC per recording (CaGr-Dx ROI active fraction: 0.79±0.06, N = 19 hemispheres; OGB1-AM ROI active fraction: 0.74±0.08, N = 11 hemispheres; p = 0.6228, t-test). Waves propagated among OGB1-AM labeled cells in the SC with a median wave front velocity of 36.11 μm/s (median absolute deviation: 13.00 μm/s, N = 189 waves), which was similar to the wave speeds observed with presynaptic recordings (CaGr-Dx mean: 42.93±1.73 μm/s, OGB1AM mean: 43.04±6.68 μm/s, p = 0.9881, t-test). Together, these results indicate that the spatiotemporal properties of presynaptic retinal waves match those of postsynaptic retinal waves measured in the SC.

We next performed high spatial resolution 2P imaging on active regions observed at low magnification. We found that calcium waves propagated among SC neurons (Fig. 2g-i) (fraction of cells active per wave, 0.48 ± 0.07; fraction of cells active in a wave during a 10 min recording, 0.87 ± 0.08; N = 787 cells, 13 waves, 3 recordings), and that the activity of nearby cells was more temporally correlated than distant cells (Fig. 2i-j) (Supplementary Fig. 5). The traveling waves among cells in the retinal input layer of the SC were completely sensitive to blockade of spiking activity in the contralateral eye (Fig. 2h and Supplementary Fig. 3) (N = 6 hemispheres; ROI active fraction: control, 0.80±0.08; TTX, 0.004±0.003), but not the ipsilateral eye (N = 2 animals, ROI active fraction: control, 1.00±0.00; TTX, 0.998±0.002). These experiments show that retinal waves drive wave-like activation patterns in retinorecipient target neurons, indicating that spontaneous activity in the retina provides a template pattern that is matched in higher order circuits in the visual system.

Waves nucleate in binocular retina and exhibit bilateral coordination

Retinal waves are thought to emerge from recurrent excitatory connections in networks of spontaneously active amacrine cells and ganglion cells[25] and are presumed to originate randomly throughout the retina. We examined the initiation sites of retinal waves *in vivo* by analyzing the calcium event response frequencies for all active ROIs at the onset of waves. Interestingly, we discovered that instead of a uniform distribution of wave initiation sites, waves preferentially nucleated in the rostral-medial SC (Fig. 3a) (N = 995 waves). Consistent with this preferential site of wave generation, waves propagated with a marked directional bias towards the caudal-lateral SC, equivalent to a directional preference for the dorsal-nasal pole of the retina (Fig. 3b) (N = 995 waves, Rayleigh test of Uniformity, p = 0). This directional bias was the same for both presynaptic and postsynaptic recordings (Supplementary Fig. 6) and was similar to but stronger than the wave direction bias reported in a recent *in vitro* study[21]. The overall preference for waves to propagate towards the dorsal-nasal retina is aligned with but directly opposite the direction preference of RGCs and visual cortical neurons at the time of eye opening[26,27], which corresponds to movement towards the ventral-temporal pole of the retina. It is possible that the pronounced wave direction bias we observed mediates the development of aspects of this directionally sensitive visual circuit. The notable preference for wave initiation in the rostral-medial SC

(Fig. 3a) indicates a corresponding site of wave generation in the ventral-temporal retina, which represents the binocular portion of the visual field in mice. This suggests that retinal waves may have an enhanced role in mediating development of binocular aspects of maps in the visual system, such as the formation of eye specific connectivity and matched orientation selectivity between the eyes.

Since retinal waves arise spontaneously, it is commonly assumed that waves in each eye are autonomous and drive their corresponding visual circuits independently, giving rise to a completely asynchronous activation pattern that could be used for segregation of eye-specific projections[6,28]. Since unilateral TTX blockade or enucleation abolished pre-synaptic and post-synaptic retinal waves (Supplementary Fig. 3), we hypothesized that the retinal waves would occur independently in the two SC hemispheres. Unexpectedly, simultaneous bilateral calcium imaging of the SC revealed that retinal waves sometimes traveled with matched spatial patterns in both hemispheres at the same time (Fig. 3c-f). These bilaterally coordinated waves were found when recording from presynaptic afferents in the SC with CaGr-Dx (Supplementary Movie 3) and from the postsynaptic networks within the SC labeled with OGB1-AM (Fig. 3c and Supplementary Movie 4). Temporally matched waves occurred throughout the SC and constituted a small (15.8%), but significant subset of all waves (p-value = 0.00098, t-test). Synchronous waves in the two hemispheres of the SC also typically propagated in a highly correlated manner spatially (85.0% of temporally correlated waves were also spatially correlated, accounting for 13.4% overall; p-value = 0.004535, t-test; Fig. 3c-e). Retinopetal projections as well as retino-retinal connectivity have been reported in the developing mammalian retina[29,30] (Supplementary Fig. 7). Thus it is possible that descending synchronized inputs or synaptic interactions between the two retinas may cause a small subset of retinal waves to initiate at matched retinotopic locations bilaterally. Since commissural connections between the hemispheres in SC and visual cortex are retinotopically coordinated[31,32] and orientation selectivity is matched between the eyes in the binocular visual cortex, even in the absence of visual experience[33], a possible function for synchronous retinal waves is to regulate bilateral matching of visual map connectivity.

Retinal waves propagate to and within visual cortex

Visual information from the retina is routed to the primary visual cortex through the dLGN of the thalamus. Retinogeniculate input to the dLGN in mice originates from collateral fibers that arise from a subset of retinocollicular afferents. Therefore, retinal waves transmitted to the SC should also be relayed to the visual cortex through the thalamus. To test whether retinal waves induce propagating waves within visual cortex, we performed simultaneous wide field calcium imaging of the SC and ipsilateral visual cortex (Fig. 4a-c). We found that traveling waves in the visual cortex were coincident with retinal waves propagating across the ipsilateral SC (Fig. 4d,e) (coactive fraction, V1/SC = 50/81 waves, N = 4 hemispheres), and interwave intervals were similar in SC and V1 (Fig. 4f) (P6-P9 SC, 40.53 ± 2.81 s, N = 133 waves; P6-P9 V1, 49.01 ± 4.79 s, N = 62 waves; p = 0.1292, t-test). The retinotopic map in primary visual cortex (V1) is mirrored and rotated with respect to the retinotopic map in the ipsilateral SC (Supplementary Fig. 8). Notably, after correcting for the mirrored and rotated maps, the direction of wave propagation in visual cortex was retinotopically matched to the direction of wave travel in the SC (Fig. 4g,h) (r = 0.835, p = 4.707e-14, Pearson's correlation, N = 50 waves). These results indicate that retinal waves carry functional information corresponding to retinal organization simultaneously throughout multiple areas of the visual system during development.

The primary visual cortex in mice contains a retinotopic map of the contralateral visual hemifield and is adjoined by up to 9 extrastriate visual areas homologous to those seen in

carnivore and primates[34], each of which contains a duplicate map of retinal topography. To gain a better understanding of the overall contribution of retinal waves to ongoing patterned activity among developing visual cortical areas in mice, we used a Cre-loxP approach (*Emx1-Cre:Ai38*) to express the genetically encoded calcium sensor GCaMP3 in all excitatory cortical neurons[35]. Widefield fluorescent GCaMP3 signals from neocortical neurons were imaged directly through the skull simultaneously with OGB1-AM signals through a cranial window over the SC (Fig. 5a,b). Retinal waves in the SC propagated concurrently with waves in the visual cortex (V1) and separate, secondary wave fronts were initiated in extrastriate cortical areas (Fig. 5c) (Supplementary Movie 5). We created maps of retinal topography in the visual cortex and midbrain by colorizing and merging dF/F image frames based on the locations of SC retinal wave fronts within 10 min recordings (Fig. 5d). This functional map of wave-based retinotopy revealed a large primary map in visual cortex that was mirrored and rotated with respect to the SC map (Fig. 5d) and which was remarkably consistent with the known visual map organization of adult mouse V1 compared with SC[34,36]. Though the frequency of calcium events was higher in V1 and extrastriate cortex relative to SC (Fig. 5e) (median ± median absolute deviation, SC: 0.010 ± 0.003 Hz; V1: 0.013 ± 0.003 Hz; extrastriate: 0.017 ± 0.003 Hz), most of the activity in V1 occurred within seconds of a retinal wave (Fig. 5f). Retinal waves also triggered activity in secondary visual cortical areas, but much of the ongoing cortical activity in extrastriate areas appeared to be independent of retinal waves (Fig. 5e-g), indicating a strong role for intra- or sub-cortical inputs separate from the primary visual pathway in driving ongoing activity within developing extrastriate cortex. Ablation of contralateral retinal input dramatically diminished spontaneous activity in the SC and V1, but in surrounding extrastriate visual areas the frequency of ongoing activity was unaffected though the spatial distribution of this activity noticeably shifted (Fig. 5e,g) (median ± median absolute deviation, SC: 0 ± 0 Hz; V1: 0.002 ± 0.002 Hz; extrastriate: 0.017 ± 0.005 Hz and Supplementary Fig. 9). These results indicate that retinal waves provide a primary source of patterned activity for V1 during early development and further modulate activity in extrastriate visual areas. Retinal waves convey patterned information suitable for driving activity-dependent development of neocortical circuits before the onset of vision and may thus prompt coordinated alignment and refinement of topographic maps across the visual system.

Retinal waves are abolished in epibatidine treated mice

Classic studies show that pharmacologic manipulation of retinal waves *in vivo* with epibatidine, a high affinity agonist for nicotinic aceytlcholine receptors, disrupts visual map development in ferret[9,10,13,37] and mouse[38,39,40]. These studies relied on *in vitro* evidence that epibatidine blocks retinal waves[9,41], but the effects of epibatidine on wave generation *in vivo* and the link between retinal waves and visual map development remain uncertain. We generated *Rx-Cre:Ai38* mice, which express the genetically encoded calcium reporter, GCaMP3, in both RGCs and forebrain neurons to perform simultaneous recordings of retinal waves in RGC axons and the visual cortex. Retinal waves propagated simultaneously in SC and V1 (Fig. 6c,d) and were completely abolished after monocular injection into the contralateral eye of 1000 μM epibatidine (Fig. 6e,f) (control, N = 58 movies, 0.96 ± 0.05 waves/min; contra epi, N = 14 movies, 0 waves/min; p = 8.2e-14, pairwise-t-test) (Supplementary Movie 6), the concentration typically used *in vivo* to examine the role of retinal waves in visual map development[13,37,38,39,40]. Surprisingly, retinal waves were also abolished in SC and V1 ipsilateral to the injected eye (Fig. 6f) (N = 14 movies, 0 waves/min; p = 8.2e-14), suggesting that at 1000 μM epibatidine could mediate some of its effects systemically. Consistent with a concentration-dependent systemic effect, monocular injection of 0.01 μM or 0.2 μM epibatidine significantly reduced wave frequency in the contralateral (0.01 μM, 0.36 ± 0.12 waves/min, N = 9 movies, p = 0.00012; 0.2 μM, 0.45 ± 0.10 waves/min, N = 12 movies, p = 0.00028, pairwise-t-test), but not ipsilateral hemisphere

(0.01 μM, 0.60 ± 0.18 waves/min, N = 9 movies, p = 0.06280; 0.2 μM, 0.82 ± 0.08 waves/min, N = 12 movies, p = 0.89135). These results are consistent with long standing evidence based on *in vitro* recordings[8] that cholinergic neurotransmission plays an essential role in generating retinal waves, and that *in vivo* manipulations with epibatidine disrupt visual map development by abolishing retinal waves throughout the visual system.

Discussion

There is substantial *in vitro* evidence for spontaneous waves of neuronal activity in the prenatal or postnatal retina of a number of vertebrate species, including rodent, ferret, and monkey[42,43]. Slow activity transients or bursting activity measured with EEG or extracellular electrodes in the dLGN and visual cortex of rat or ferret *in vivo* before eye opening are modulated by retinal input and therefore believed to be driven by retinal waves[18,24,44]. These slow activity transients are homologous to the slow activity EEG transients recorded in preterm human fetal occipital cortex[45,46]. Since these self-organized patterns of spontaneous activity are present before the onset of patterned vision, it has long been hypothesized that retinal waves may help organize aspects of visual circuit function that are established before visual experience, such as maps for orientation[33,47], direction[27], and ocular dominance[33,48].

Our recordings in mouse pups aged P3-P9 indicate that spontaneous retinal waves are present for at least a week of development *in vivo* and exhibit a pattern of activity appropriate for communicating retinal organization to circuits throughout the visual system. Imaging of RGC afferents or SC neurons together with simultaneous imaging in V1 demonstrates that retinal waves generate matched activity patterns in the midbrain and cortex, supporting the hypothesis that emergent retinal activity mediates the development of linked visual circuitry within and across multiple neocortical and subcortical brain regions[49].

Retinal waves *in vivo* exhibited a number of properties that could not have been predicted based on previous *in vitro* recordings, including a preferential site of generation in the ventral-temporal retina, a biased direction of wave travel towards the dorsal-nasal retina, and a differential role in driving primary versus secondary visual cortical activities (see also Supplementary Discussion). Surprisingly, we also found that a significant subset of retinal waves exhibited coordinated patterns across both hemispheres. This suggests that bilateral retinal waves could help establish interhemispheric connections, a role not previously ascribed to waves. Moreover, the remarkable mirror symmetric pattern of ocular dominance columns between hemispheres observed in some monkeys[50], which are difficult to explain based on the presumed random pattern of waves between the eyes, may be better understood in the context of the clearly non-random nature of waves across the two hemispheres found *in vivo*.

A causal link between retinal waves and visual map development has been difficult to definitively establish, partly due to the lack of evidence for wave generation and propagation *in vivo.* Our experiments show that pharmacological manipulations that were previously shown to profoundly disrupt visual map development[9,10,13,37,38,39] also block wave generation *in vivo*, strengthening the causal link between wave activity and map development.

Given the remarkable fidelity of retinal waves during the period prior to eye opening in mice we report here *in vivo*, together with previous work demonstrating that spontaneous waves within macaque retina are present *in vitro* before birth[43], it seems likely that the visual system experiences patterned activation by retinal waves for a substantial gestational period

during human fetal development that may be crucial for shaping the functional maturation of neural circuits before the onset of sensory experience.

METHODS

Animals

Animal care and use was performed in compliance with the Yale IACUC, U. S. Department of Health and Human Services and Institution guidelines. Neonatal wild type mice (C57BL/6J) and Ai38 floxed GCaMP3 reporter mice (JAX no. 014538)[35] crossed with *Emx1-Cre* mice (JAX no. 005628) or *Rx-Cre*[51] aged 1-9 days after birth (P1-P9) were used.

Anterograde calcium indicator labeling

For presynaptic calcium imaging experiments, 20% w/v Calcium Green-1 Dextran (3000 MW, Invitrogen, C6765) in saline was prepared and injected into the retinas of P1-P3 mice that were deeply anesthetized on ice following previously published protocols[52]. After injection of ~0.5 μL per eye, five square-wave 100 ms pulses of 25V with 900 ms interval were applied directly across each eye in both directions using methods similar to those previously published for DNA plasmid delivery[53]. After electroporating each eye alone, whole-head electroporation was applied over both eyes with five 75V, 100ms square wave pulses and 900 ms interval in each direction. The animal was then given topical anesthetic over each eye and allowed to wake and recover on a heating pad before being returned to the dam. This technique results in a labeled population of RGCs distributed across the majority of the retina and noticeable anterograde labeling of RGC axon terminal arbors in the superior colliculus within 2 days of injection (Fig. 1a).

Surgical procedure for in vivo imaging

Mice aged P3-P9 were deeply anesthetized with isoflurane (2.5%) in oxygen and then placed on a heating pad set to 36.5°C via a homoeothermic temperature monitor (NPI TC-20, ALA Scientific). Local anesthesia was produced by subcutaneous injection (0.05 ml) of 1% Xylocaine (10 mg/ml lidocaine/0.01 mg/ml epinephrine, AstraZeneca) under the scalp. After removal of the scalp, steel head posts were fixed to the anterior and posterior portions of the exposed skull using cyanoacrylate glue. Isoflurane anesthesia was adjusted between 0.5-1.0% as necessary to maintain a stable respiratory rate. A ~2 mm oval craniotomy was created by gentle etching into interparietal skull and removing the resulting bone flap above the superior colliculus, just posterior to lambda using the tip of an 18G syringe needle. After achieving hemostasis, the dura was carefully removed using forceps and microdissection scissors. The craniotomy was filled with warm (37°C) low temperature melt agarose (A9414, Sigma, 1.5% in sterile buffered saline, 150mM NaCl, 2.5 mM KCl, 10 mM HEPES, pH 7.4).

Cellular bulk loading with a calcium sensitive dye

Loading neurons *in vivo* with the calcium indicator Oregon Green BAPTA-1-AM (OGB1-AM; Invitrogen) was performed using standard procedures similar to those described previously[54,55]. Dye was prepared by dissolving 50 μg of OGB1-AM in 4 μl 20% pluronic acid in DMSO (Invitrogen) and 35 μl of sterile buffered saline (150 mM NaCl, 2.5 mM KCl, 10 mM HEPES, pH 7.4) and 1 μl of 10 mM Alexa 594 hydrazide (Invitrogen) and sonicating for 20 min. The solution was then filtered through a 0.45 μm microcentrifuge filter (Millipore).

Pulled glass micropipettes (1B150F-4; World Precision Instruments) were loaded with OGB1-AM dye solution, and inserted into an electrode holder connected to a Picospritzer III

(General Valve Corp) set to an output pressure of 10 psi. Bulk labeling with OGB1-AM[56] was achieved at 2-4 injection sites per hemisphere by lowering the pipette to a depth of 100-300 μm below the pial surface of the superior colliculus or primary visual cortex with a motorized micromanipulator (MP-225, Sutter) and delivering 60 brief (20 msec) pressure pulses over the course of 2 min. A circular, 5 mm diameter #1.5 coverglass (Warner Instruments) was placed over the craniotomy in fresh agarose and stabilized with Kwik-Sil (World Precision Instruments).

In-vivo calcium imaging

A 1 hr recovery period in the dark under continuously delivered medical oxygen with isoflurane at 0% was allowed after craniotomy surgery and dye injection was completed. This recovery period was the typical minimum time required for spontaneous waves of activity to develop in the visual system after the cessation of deep anesthesia. Spontaneous waves occurred only in unanesthetized mouse pups (26/30 unanesthetized mice at 0% isoflurane; 0/11 anesthetized mice ≥ 0.25% isoflurane, $p = 6.099e\text{-}06$) (Supplementary. Fig. 4). During the recordings, the head was fixed under the microscope objective by steel posts attached to the skull and the body was loosely surrrounded by cotton gauze, such that the animals could move freely on the heating pad. During the experiment, mouse pups spent the majority of time in a quiet, resting state interrupted by brief motor twitches of limbs or tail.

A two-photon microscope system (Ultima IV, Prairie Technologies) was used to image the calcium dyes. A Ti:Sapphire laser (Mai Tai, Spectra-Physics) was tuned to 800 nm for excitation of OGB1-AM and Calcium Green-1 Dextran. Total power delivered to the brain was <50 mW. Imaging was performed using a 20X/1.0NA saline-immersed objective (#421452-9900, Zeiss). Image frames corresponding to a field of view of 550 × 550 μm or 225 × 225 μm or 138 × 138 μm were acquired at a rate of 1.2 Hz, 7.5 Hz, or 22.3 Hz respectively. Each recording consisted of a single, continuously acquired movie during a period of 10min.

For wide field calcium imaging, a CCD camera (Pixelfly, The COOKE Corporation) coupled to an Olympus BX51 and a 5X/0.25NA objective (#440125, Zeiss) or 2.5x 0.075NA objective (Zeiss #440310-9903) was used to image calcium responses in both hemispheres of the superior colliculus simultaneously or a collicular hemisphere and the ipsilateral visual cortex simultaneously. Epifluorescent illumination was provided by a Hg^{2+} light source (X-Cite Series 120, EXFO) through a neutral density filter and a filter cube set (U-MGFPHQ, Olympus) with the minimum illumination intensity that still gave detectable calcium signals using a CCD exposure of 200 msec.

Ablation of retinal input

To abolish retinal activity, the animal was reanesthetized under 2.5% isoflurane and the eye lid surgically opened with 1% xylocaine applied to the eye. For enucleation, the eye was surgically removed and 1% xylocaine applied to the orbit. For eye injections, 0.5 - 1 μl of 10 μM tetrodotoxin (TTX; Tocris #1069) or (±)-Epibatidine dihydrochloride hydrate (10 nM, 200 nM, or 1 mM; Sigma #E1145) dissolved in saline was pressure injected using a glass micropette inserted into the vitreous. After completion of the enucleation or eye injection, the animal was returned to 0% isoflurane with total procedure time under deep anesthesia <10 min.

Calcium signal detection

Image processing and calcium signal detection was performed using custom software routines written in MATLAB (Mathworks, Natick, MA). For low magnification 2P imaging movies or wide field CCD movies, a rectangular grid of ROIs (for each ROI; h =45 μm, w =

45 μm) was masked over the average image, *F0*, of visible calcium indicator fluorescence for each hemisphere of a movie. For cell based analysis in higher magnification 2P imaging movies, a motion correction algorithm described previously[57] was first applied to the movie to correct for small xy displacements within the focal plane of the movie due to cardiopulmonary or twitch based movements. Unambiguous cell contours were semi-automatically identified in the average image, *F0*, for cell based movies and an ROI mask created inside each cell. Calcium signals for each ROI was the average fluorescence intensity inside each ROI in each frame, *Ft*, measured as a function of time ($dF/F = (Ft - F0)/F0$). Calcium transients were detected using automatic unbiased detection routines to identify local maxima (>2 standard deviations of the derivative of the signal). Image frames containing z-artifacts were identified as frames recorded during periods of time when a decrement or increment in fluorescence occurred in 100% of the ROI population spanning 2 frames or less, and were excluded from calcium event detection. Calcium event onsets were set as the first frame in the rising phase of the signal. Event offsets were set as the half-amplitude decay time for each calcium transient.

Wave detection

A waveform representing the population activity for each movie was constructed by smoothing the envelope of the population activity histogram for each movie with a 10 order Hanning filter. Local maxima separated by greater than 10 secs and having rising phase onsets surpassing a 5% population activity threshold from the local minima were set as wave peak and onset times respectively. The time between the wave peak and the next local minima when population activity during the falling phase decreased to less than 20% was set as the wave offset. Each wave period was then interactively confirmed based on the visually detected waves in the raw movie data. Any detected calcium transients occurring outside of wave periods were excluded from further analysis.

To detect wavefronts, an array of spike times (calcium event onsets) for each wave was constructed by creating an *M*x*N*x*P* array where *M*x*N* equals the X,Y dimensions of the movie image and *P* equals the number of frames within a wave. A binary mask for each ROI exhibiting a calcium spike during a wave was created at the corresponding time within the array for the wave to represent individual spike times. A binary dilation/erosion operation using a structuring element with a height and width 3 pixels larger than the height and width of the ROI contours was then convolved over each wave frame in the spike array and any 8-neighbor connected components in each binary frame that were less than two ROI contour areas in size were discarded. To calculate the wave front position for each frame within the spike array for the wave, a structuring element 2.5x larger in height and width than each ROI was used to perform a binary dilation of the frame. The centroid location of the binary connected components within the resulting spike frame was then taken to be the wavefront location for that frame.

For each wave, a single merged wave frame was created by making a maximum projection along the dimension *P* of the binary wave spike array. The wave area was the sum of non-zero areas within the merged wave frame and the major axis length of the largest 8-neighbor connected component within the merged wave frame was taken to be the distance for that wave. The active fraction for each wave of each hemisphere was the number of ROIs participating in a wave divided by the total number of ROIs in that recording. The active fraction for each hemisphere was the total number of ROIs active at least once during a recording divided by the total number of ROIs. Wave speeds were determined by finding the set of distances for each wave frame's centroid relative to the wave onset centroid and calculating the mean of this set. Wave directions were determined by calculating the vector sum of the iterative directions between wave front centroids in sequential frames for each

wave and were interactively corrected if the automatically calculated wave direction was off by more than $\pi/4$ radians from the visually discerned wave angle. Measured wave directions in the left hemisphere were mirrored so that the direction values could be directly compared between hemispheres. Wave frequencies for each recording were calculated as the number of waves divided by the length of time for each recording. Interwave intervals for each recording were calculated as the set of time intervals between the onsets of sequential waves in each recording.

Data analysis

Data sets were analyzed using custom routines written in MATLAB (The Mathworks, Natick, MA) and in R (The R Project for Statistical Computing, http://www.r-project.org). To quantify temporal correlations between cells within a recording, cross-correlation values within a calcium event onset window of +/− 100 ms or +/− 1 frame for each pair of cells in a network was calculated. Interval reshuffling was then performed as described previously[58]. The significance of cross-correlation values for real datasets was determined through comparison with distributions calculated from the randomized datasets using a threshold significance level of $p < 0.05$. The distribution of pairwise cell correlations as a function of distance was normalized to the distribution of all pairwise cell distances to determine the relative pairwise cell correlation probability density (Supplementary Fig. 5). Distribution means were compared using two-sample Student's t-Tests or using ANOVA followed by pairwise-t-tests with Holm correction when analyzing the effects of multiple grouping factors ($p < 0.05$ set as significance). Values are reported as means with the standard error of the mean or medians with the median absolute deviation.

Peri-event time histograms were calculated using wave onset times as the stimulus trigger for every ROI of a movie, using an interval window of [−1000, 15000 ms] around each wave time to find the set of detected calcium transient onsets. The normalized response frequency for each ROI was calculated as the total number of detected calcium onsets divided by the number of stimulus triggers for each recording. For each ROI of each hemisphere, the normalized anterior-posterior and medial-lateral distances were calculated as the ROI centroid *x* and *y* distances from the most anterior-medial location in the dye labeled craniotomy image normalized to the most posterior and lateral locations in the dye labeled craniotomy image.

For comparison of wave directions in the SC and VCtx, wave directions in VCtx were matched to the SC retinotopic map by mirroring and rotating the measured VCtx wave angles as shown in Supplementary Fig. 8.

To quantify the temporal and spatial correlations of retinal waves occurring at the same time in both hemispheres, the distribution of interwave onset intervals in Supplementary Fig. 1 was fitted to a gamma distribution and the resulting shape (2.5177) and rate (0.0387) parameters from the observed distribution were used to generate sequences of random wave intervals to which the observed wave interval sequences were compared. For each recording, the observed sequences of wave interval onset times for the two hemispheres was smoothed with a gaussian (sigma = 3 s). A cross-correlation value was then calculated between these two smoothed wave interval ‘spike’ trains and compared with a distribution of cross-correlation values calculated from 1000 random wave onset simulations that consisted of one sequence of observed wave onsets and one sequence of random wave intervals. Overlapping wave onsets observed in a recording were determined to be significantly temporally correlated if the observed cross-correlation value exceeded 95% of the simulated temporal cross-correlation values.

For determining bilateral spatial correlations, a database of image masks for 2.5x CCD recordings was created for every frame between the onset and offset of each wave by segmenting the raw dF/F image using Otsu's method. For each wave pair with overlapping wave onsets, the wave image mask for one hemisphere was flipped and a 2D cross-correlation was computed between the two hemispheres for each frame of a bilateral wave. The maximum value in the 2D correlation image was used to calculate the estimated *x, y* displacements between the wave masks for the two hemispheres. A set of Euclidean Distances was calculated from the *x, y* displacement to the location of the 2D autocorrelation value for one of the hemispheres for each wave frame (center of the wave mask image) and then the mean Euclidean distance was taken as an observed Spatial Similarity Metric (SSM) for that wave pair. A second SSM was also calculated for each wave pair by calculating the Mahalanobis Distance from a set of pattern vectors for the wave masks in each hemisphere, where the input pattern vector is a *M*x*N* array, where for each frame, *M*, a set of *N* pattern metrics was calculated that included the *x, y* displacement values from the 2D correlation, a set of wave mask image texture descriptors (functions *graycoprops, statxture,* and *invmoments* from[59]), and a set of regional measurements from the largest component in the binary wave mask (Area, Centroid, Eccentricity, EquivDiameter, Extent, MajorAxisLength, MinorAxisLength, Orientation, and Solidity from function *regionprops*, MATLAB Image Processing Toolbox). For each recording, if the simulated temporal correlation value exceeded the observed temporal correlation value, then for each overlapping wave pair a random wave from the wave mask database was aligned to the anterior-medial point of the SC for one of the observed wave masks and then the random SSMs were calculated. An observed wave pair was spatially correlated if <1% of the random wave pairs had SSMs less than or equal to the observed SSMs for that wave pair.

Supplementary Material

Refer to Web version on PubMed Central for supplementary material.

Acknowledgments

We thank R. Sachdev and D. McCormick for *Emx1-Cre:Ai38* mice, C. Chen for helpful advice on ganglion cell loading with calcium indicators, and Y. Zhang for technical support. We would like to thank M. Colonnese and members of the Crair lab for valuable comments on the manuscript. This work was supported by NIH grants P30 EY000785 and R01 EY015788 to M.C.C., support from T32 NS007224 to J.A., and support from T15 LM070506 and T32 EY017353 to T.B.. M.C.C. also thanks the family of William Ziegler III for their support.

REFERENCES

1. Buffelli M, Burgess RW, Feng G, Lobe CG, Lichtman JW, Sanes JR. Genetic evidence that relative synaptic efficacy biases the outcome of synaptic competition. Nature. 2003; 424:430–4. [PubMed: 12879071]
2. Marder E, Rehm KJ. Development of central pattern generating circuits. Curr Opin Neurobiol. 2005; 15:86–93. [PubMed: 15721749]
3. Petersson P, Waldenström A, Fåhraeus C, Schouenborg J. Spontaneous muscle twitches during sleep guide spinal self-organization. Nature. 2003; 424:72–5. [PubMed: 12840761]
4. Sanes JR, Lichtman JW. Development of the vertebrate neuromuscular junction. Annu Rev Neurosci. 1999; 22:389–442. [PubMed: 10202544]
5. Katz LC, Shatz CJ. Synaptic activity and the construction of cortical circuits. Science. 1996; 274:1133–8. [PubMed: 8895456]
6. Meister M, Wong RO, Baylor DA, Shatz CJ. Synchronous bursts of action potentials in ganglion cells of the developing mammalian retina. Science. 1991; 252:939–943. [PubMed: 2035024]
7. Wong RO, Meister M, Shatz CJ. Transient period of correlated bursting activity during development of the mammalian retina. Neuron. 1993; 11:923–38. [PubMed: 8240814]

8. Feller MB, Wellis DP, Stellwagen D, Werblin FS, Shatz CJ. Requirement for cholinergic synaptic transmission in the propagation of spontaneous retinal waves. Science. 1996; 272:1182–7. [PubMed: 8638165]
9. Penn AA, Riquelme PA, Feller MB, Shatz CJ. Competition in retinogeniculate patterning driven by spontaneous activity. Science. 1998; 279:2108–2112. [PubMed: 9516112]
10. Stellwagen D, Shatz CJ. An instructive role for retinal waves in the development of retinogeniculate connectivity. Neuron. 2002; 33:357–367. [PubMed: 11832224]
11. McLaughlin T, Torborg CL, Feller MB, O'Leary DDM. Retinotopic map refinement requires spontaneous retinal waves during a brief critical period of development. Neuron. 2003; 40:1147–1160. [PubMed: 14687549]
12. Chandrasekaran AR, Plas DT, Gonzalez E, Crair MC. Evidence for an instructive role of retinal activity in retinotopic map refinement in the superior colliculus of the mouse. J Neurosci. 2005; 25:6929–38. [PubMed: 16033903]
13. Huberman AD, Speer CM, Chapman B. Spontaneous retinal activity mediates development of ocular dominance columns and binocular receptive fields in v1. Neuron. 2006; 52:247–254. [PubMed: 17046688]
14. Chalupa LM. Retinal waves are unlikely to instruct the formation of eye-specific retinogeniculate projections. Neural Dev. 2009; 4:25. [PubMed: 19580684]
15. Feller MB. Retinal waves are likely to instruct the formation of eye-specific retinogeniculate projections. Neural Dev. 2009; 4:24. [PubMed: 19580682]
16. Maffei L, Galli-Resta L. Correlation in the discharges of neighboring rat retinal ganglion cells during prenatal life. Proc Natl Acad Sci U S A. 1990; 87:2861–2864. [PubMed: 2320593]
17. Hanganu IL, Ben-Ari Y, Khazipov R. Retinal waves trigger spindle bursts in the neonatal rat visual cortex. J Neurosci. 2006; 26:6728–36. [PubMed: 16793880]
18. Colonnese MT, Khazipov R. “Slow activity transients” in infant rat visual cortex: a spreading synchronous oscillation patterned by retinal waves. J Neurosci. 2010; 30:4325–37. [PubMed: 20335468]
19. Hofbauer A, Dräger UC. Depth segregation of retinal ganglion cells projecting to mouse superior colliculus. J Comp Neurol. 1985; 234:465–74. [PubMed: 3988995]
20. Bansal A, Singer JH, Hwang BJ, Xu W, Beaudet A, Feller MB. Mice lacking specific nicotinic acetylcholine receptor subunits exhibit dramatically altered spontaneous activity patterns and reveal a limited role for retinal waves in forming ON and OFF circuits in the inner retina. J Neurosci. 2000; 20:7672–81. [PubMed: 11027228]
21. Stafford BK, Sher A, Litke AM, Feldheim DA. Spatial-temporal patterns of retinal waves underlying activity-dependent refinement of retinofugal projections. Neuron. 2009; 64:200–12. [PubMed: 19874788]
22. Ford KJ, Félix AL, Feller MB. Cellular mechanisms underlying spatiotemporal features of cholinergic retinal waves. J Neurosci. 2012; 32:850–63. [PubMed: 22262883]
23. Mooney R, Penn AA, Gallego R, Shatz CJ. Thalamic relay of spontaneous retinal activity prior to vision. Neuron. 1996; 17:863–874. [PubMed: 8938119]
24. Weliky M, Katz LC. Correlational structure of spontaneous neuronal activity in the developing lateral geniculate nucleus in vivo. Science. 1999; 285:599–604. [PubMed: 10417392]
25. Blankenship AG, Feller MB. Mechanisms underlying spontaneous patterned activity in developing neural circuits. Nat Rev Neurosci. 2010; 11:18–29. [PubMed: 19953103]
26. Elstrott J, Anishchenko A, Greschner M, Sher A, Litke AM, Chichilnisky EJ, Feller MB. Direction selectivity in the retina is established independent of visual experience and cholinergic retinal waves. Neuron. 2008; 58:499–506. [PubMed: 18498732]
27. Rochefort NL, Narushima M, Grienberger C, Marandi N, Hill DN, Konnerth A. Development of direction selectivity in mouse cortical neurons. Neuron. 2011; 71:425–32. [PubMed: 21835340]
28. Zhang J, Ackman JB, Xu H-P, Crair MC. Visual map development depends on the temporal pattern of binocular activity in mice. Nat Neurosci. 2011; 15:298–307. [PubMed: 22179110]
29. Gastinger MJ, Tian N, Horvath T, Marshak DW. Retinopetal axons in mammals: emphasis on histamine and serotonin. Curr Eye Res. 2006; 31:655–67. [PubMed: 16877274]

30. Müller M, Holländer H. A small population of retinal ganglion cells projecting to the retina of the other eye. An experimental study in the rat and the rabbit. Exp Brain Res. 1988; 71:611–7. [PubMed: 3416972]
31. Takahashi M, Sugiuchi Y, Shinoda Y. Commissural mirror-symmetric excitation and reciprocal inhibition between the two superior colliculi and their roles in vertical and horizontal eye movements. J Neurophysiol. 2007; 98:2664–82. [PubMed: 17728384]
32. Lewis JW, Olavarria JF. Two rules for callosal connectivity in striate cortex of the rat. J Comp Neurol. 1995; 361:119–37. [PubMed: 8550874]
33. Crair MC, Gillespie DC, Stryker MP. The role of visual experience in the development of columns in cat visual cortex. Science. 1998; 279:566–70. [PubMed: 9438851]
34. Wang Q, Burkhalter A. Area map of mouse visual cortex. J Comp Neurol. 2007; 502:339–57. [PubMed: 17366604]
35. Zariwala HA, Borghuis BG, Hoogland TM, Madisen L, Tian L, De Zeeuw CI, Zeng H, Looger LL, Svoboda K, Chen T-W. A Cre-dependent GCaMP3 reporter mouse for neuronal imaging in vivo. J Neurosci. 2012; 32:3131–41. [PubMed: 22378886]
36. Drager UC, Hubel DH. Topography of visual and somatosensory projections to mouse superior colliculus. J Neurophysiol. 1976; 39:91–101. [PubMed: 1249606]
37. Huberman AD, Stellwagen D, Chapman B. Decoupling eye-specific segregation from lamination in the lateral geniculate nucleus. J Neurosci. 2002; 22:9419–29. [PubMed: 12417667]
38. Rossi FM, Pizzorusso T, Porciatti V, Marubio LM, Maffei L, Changeux JP. Requirement of the nicotinic acetylcholine receptor beta 2 subunit for the anatomical and functional development of the visual system. Proc Natl Acad Sci U S A. 2001; 98:6453–8. [PubMed: 11344259]
39. Pfeiffenberger C, Cutforth T, Woods G, Yamada J, Rentería RC, Copenhagen DR, Flanagan JG, Feldheim DA. Ephrin-As and neural activity are required for eye-specific patterning during retinogeniculate mapping. Nat Neurosci. 2005; 8:1022–7. [PubMed: 16025107]
40. Rebsam A, Petros TJ, Mason CA. Switching retinogeniculate axon laterality leads to normal targeting but abnormal eye-specific segregation that is activity dependent. J Neurosci. 2009; 29:14855–63. [PubMed: 19940181]
41. Sun C, Speer CM, Wang G-Y, Chapman B, Chalupa LM. Epibatidine application in vitro blocks retinal waves without silencing all retinal ganglion cell action potentials in developing retina of the mouse and ferret. J Neurophysiol. 2008; 100:3253–-3263. [PubMed: 18922954]
42. Wong RO. Retinal waves and visual system development. Annu Rev Neurosci. 1999; 22:29–47. [PubMed: 10202531]
43. Warland DK, Huberman AD, Chalupa LM. Dynamics of spontaneous activity in the fetal macaque retina during development of retinogeniculate pathways. J Neurosci. 2006; 26:5190–7. [PubMed: 16687510]
44. Chiu C, Weliky M. Spontaneous activity in developing ferret visual cortex in vivo. J Neurosci. 2001; 21:8906–-8914. [PubMed: 11698602]
45. Vanhatalo S, Palva JM, Andersson S, Rivera C, Voipio J, Kaila K. Slow endogenous activity transients and developmental expression of K+-Cl- cotransporter 2 in the immature human cortex. Eur J Neurosci. 2005; 22:2799–804. [PubMed: 16324114]
46. Tolonen M, Palva JM, Andersson S, Vanhatalo S. Development of the spontaneous activity transients and ongoing cortical activity in human preterm babies. Neuroscience. 2007; 145:997–1006. [PubMed: 17307296]
47. Wiesel TN, Hubel DH. Ordered arrangement of orientation columns in monkeys lacking visual experience. J Comp Neurol. 1974; 158:307–-318. [PubMed: 4215829]
48. Rakic P. Prenatal genesis of connections subserving ocular dominance in the rhesus monkey. Nature. 1976; 261:467–-471. [PubMed: 819835]
49. Triplett JW, Owens MT, Yamada J, Lemke G, Cang J, Stryker MP, Feldheim DA. Retinal input instructs alignment of visual topographic maps. Cell. 2009; 139:175–85. [PubMed: 19804762]
50. Adams DL, Horton JC. Capricious expression of cortical columns in the primate brain. Nat Neurosci. 2003; 6:113–4. [PubMed: 12536211]

51. Swindell EC, Bailey TJ, Loosli F, Liu C, Amaya-Manzanares F, Mahon KA, Wittbrodt J, Jamrich M. Rx-Cre, a tool for inactivation of gene expression in the developing retina. Genesis. 2006; 44:361–3. [PubMed: 16850473]
52. Kreitzer AC, Gee KR, Archer EA, Regehr WG. Monitoring presynaptic calcium dynamics in projection fibers by in vivo loading of a novel calcium indicator. Neuron. 2000; 27:25–32. [PubMed: 10939328]
53. Dhande OS, Crair MC. Transfection of mouse retinal ganglion cells by in vivo electroporation. J Vis Exp. 2011
54. Stosiek C, Garaschuk O, Holthoff K, Konnerth A. In vivo two-photon calcium imaging of neuronal networks. Proc Natl Acad Sci U S A. 2003; 100:7319–24. [PubMed: 12777621]
55. Kerr JND, Greenberg D, Helmchen F. Imaging input and output of neocortical networks in vivo. Proc Natl Acad Sci U S A. 2005; 102:14063–8. [PubMed: 16157876]
56. Garaschuk O, Milos R-II, Konnerth A. Targeted bulk-loading of fluorescent indicators for two-photon brain imaging in vivo. Nat Protoc. 2006; 1:380–6. [PubMed: 17406260]
57. Greenberg DS, Kerr JND. Automated correction of fast motion artifacts for two-photon imaging of awake animals. J Neurosci Methods. 2009; 176:1–15. [PubMed: 18789968]
58. Cossart R, Aronov D, Yuste R. Attractor dynamics of network UP states in the neocortex. Nature. 2003; 423:283–8. [PubMed: 12748641]
59. Gonzalez RC, Woods RE, Eddins SL. Digital Image processing using MATLAB. 2009

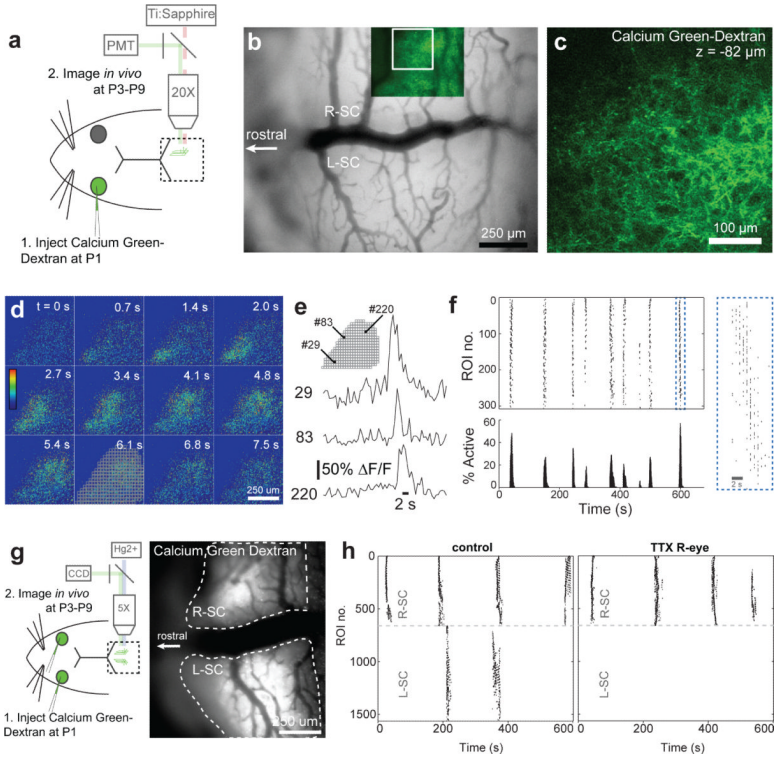

Figure 1. Spontaneous waves of activity in retinal ganglion cell arbors *in vivo*

a, Calcium dye labeling and 2P imaging. **b**, Superior colliculus (SC) craniotomy from a P5 mouse overlaid with the corresponding 2P excitation image of CaGr-Dx labeled RGC axon arbors. **c**, Higher magnification image of CaGr-Dx labeled RGC axons from inset in b, 82 μm below pial surface. **d**, Montage (dF/F) of a spontaneous wave recorded in RGC axon arbors. From same labeled field shown in b. **e**, Calcium transients from RGC axon arbors during the wave shown in d. **f**, Raster plot and activity histogram from a 677 s recording. Points indicate calcium transient onsets from individual ROIs. Same wave from d shown on right at expanded time scale. **g**, Dye labeling and wide field CCD imaging for bilateral recordings. **h**, Raster plots from animal shown in g. Intraocular TTX application blocks waves in the contralateral hemisphere.

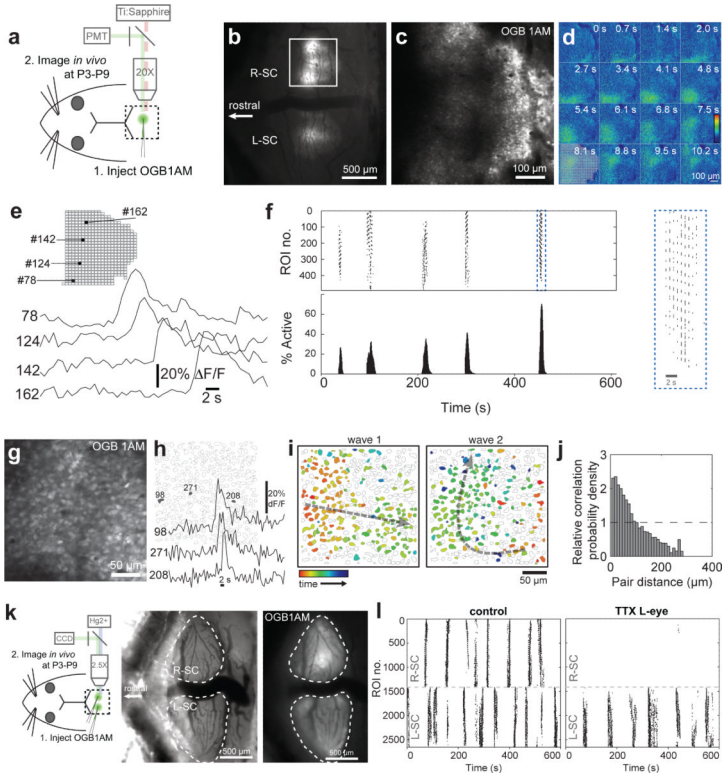

Figure 2. Spontaneous waves of correlated activity among SC neurons *in vivo*

a, Experimental overview. **b**, OGB1-AM bulk loading in the SC at P4. **c**, 2P excitation image of OGB1-AM labeled cells from inset in b, 56 µm below pial surface. **d**, Montage (dF/F) of a spontaneous wave recorded in the SC. From same labeled field shown in c. **e**, Calcium transients in local ROIs during the wave shown in d. **f**, Raster plot and activity histogram during a 610 s recording. From same experiment as d, e. **g**, Calcium imaging in single SC cells loaded with OGB1-AM. **h**, Single cell ROIs and calcium transients during a wave. **i**, Plot of neurons active during 2 sequential waves. **j**, Pairwise cell correlations as a function of pair distance. Dashed line indicates the chance distribution. **k**, Bilateral dye labeling and example widefield CCD image. **l**, Raster plots from a bilateral SC recording. Intraocular TTX application blocks waves in the contralateral hemisphere.

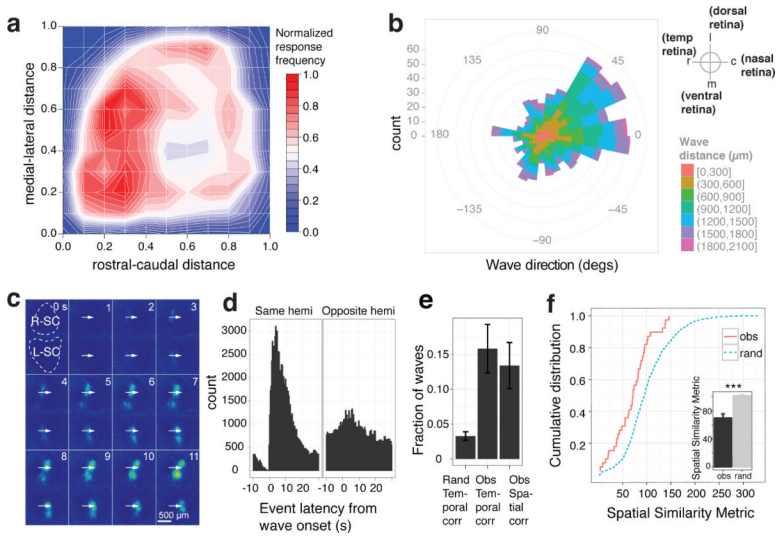

Figure 3. Retinal waves originate in the ventro-temporal retina and propagate bilaterally

a, Contour map of normalized ROI response frequencies in the SC within 2 s of wave onset. **b**, Wind rose histogram of all wave directions in SC. **c**, Montage (dF/F) of synchronized retinal waves recorded in OGB1-AM labeled cells in both hemispheres of the SC. **d**, Peri-event time histograms of calcium event latencies relative to wave onset for same or opposite hemispheres. ROI event latencies: Same hemi, N = 103354; Opposite hemi, N = 97280. **e**, Fraction of presynaptic and postsynaptic waves having significant temporal (CaGr-Dx: 52/332 waves; OGB1-AM: 20/90 waves) and spatial (CaGr-Dx: 46/332 waves; OGB1-AM: 16/90 waves) correlations bilaterally. Error bars denote s.e.m. **f**, Cumulative distributions of the spatial similarity metric across hemispheres for observed wave pairs and random wave pairs.

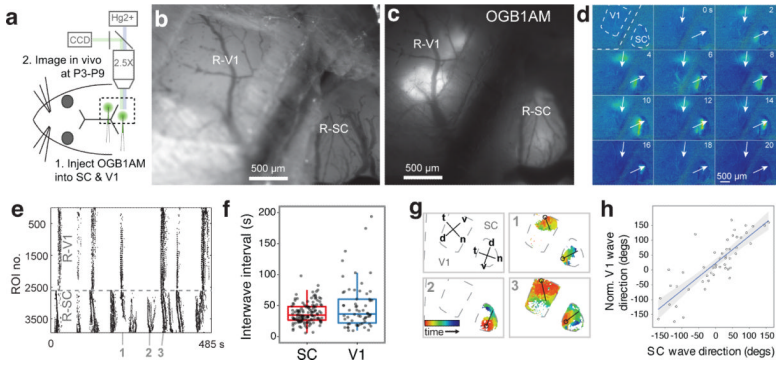

Figure 4. Retinal waves propagate simultaneously in the SC and visual cortex

a, Experimental overview. **b**, Right visual cortex (R-V1) and SC (R-SC) craniotomies from a P9 mouse. **c**, OGB1-AM bulk loading in V1 and SC. **d**, Montage (dF/F) of spontaneous waves recorded in SC and V1 simultaneously. **e**, Raster plot from the recording in d. **f**, Boxplots show interval between successive wave onsets in SC and V1 between P6-P9. **g**, Activity maps showing the direction of wave propagation for 3 waves in V1 and SC indicated in e. Top left panel shows the approximate retinotopy of mouse primary visual cortex (V1) and SC. t, temporal, n, nasal, d, dorsal, v, ventral. **h**, Plot of SC retinal wave directions versus V1 wave directions normalized to SC coordinates, with linear regression (blue line) and 95% confidence intervals (grey shading).

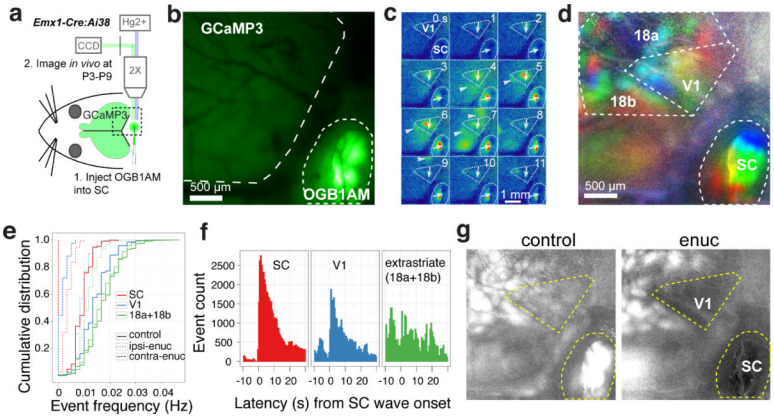

Figure 5. Retinal wave driven activity in V1 and extrastriate visual areas

a, Experimental overview. **b**, Image of transcranial cortical GCaMP3 expression and OGB1-AM bulk loading in SC of a P6 *Emx1-Cre:Ai38* mouse. **c**, Montage (dF/F) of a retinal wave recorded in SC and V1 simultaneously from same recording as in b. Arrows indicate direction and distance of wave travel, arrowheads indicate activations in V2. **d**, Topographic maps colorized by SC retinal wave front position reveal putative boundaries of V1 and secondary visual areas (Areas 18a and 18b) from same animal as in c. **e**, Cumulative distributions of calcium event frequencies before (control) and after ablation of contralateral (enuc-contra) or ipsilateral (enuc-ipsi) eye. SC, N = 2862 ROIs; V1, N = 3490 ROIs; extrastriate, 7717 ROIs. **f**, Peri-event time histograms of calcium event latencies relative to SC wave onset. SC, N = 52,284 events; V1, N = 38,244 events; extrastriate, N = 49,363 events. **g**, Max dF/F intensity projections from 10 min recordings before and after contralateral eye enucleation. From same recording as in d.

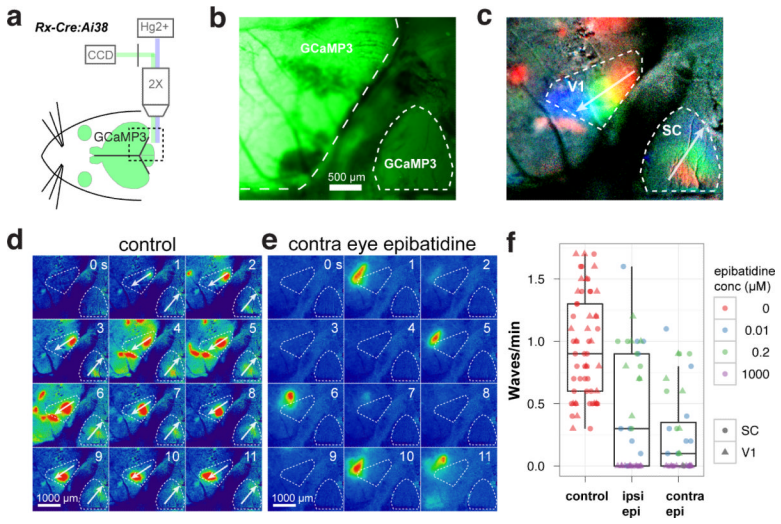

Figure 6. Retinal waves depend on cholinergic neurotransmission

a, Experimental overview. **b**, Image of transcranial cortical GCaMP3 expression and RGC axon GCaMP3 expression in SC in a P4 *Rx-Cre:Ai38* mouse. **c**, Topographic maps colorized by SC retinal wave front position for a single retinal wave simultaneously propagating in SC and V1. **d**, Montage (dF/F) of a single retinal wave from same recording as in c. **e**, Montage (dF/F) showing typical activity patterns in visual cortex after contralateral injection of 1 mM epibatidine, from same experiment as d. **f**, Box plots showing retinal wave frequency in 10 min recordings before (control) and after epibatidine injection into contralateral (contra epi; p = 2.2e-12 vs control, pairwise-t-test) or ipsilateral (ipsi epi; , p = 7.3e-08 vs control) eye in 6 mice between P2-P5.